Taylor & Francis
Taylor & Francis Group

Journal of Taibah University for Science

ISSN: (Print) (Online) Journal homepage: www.tandfonline.com/journals/tusc20

Customized structural and mechanical characteristics of Eu^{3+} imbued boro-telluro-dolomite glasses: effect of Dy^{3+} co-doping

Ibrahim Bulus, Areej S. Alqarni, Abd Rahman Tamuri, S. K. Ghoshal, Ibrahim Mohammed Danmallam & Abdullahi Anderson Kassimu

To cite this article: Ibrahim Bulus, Areej S. Alqarni, Abd Rahman Tamuri, S. K. Ghoshal, Ibrahim Mohammed Danmallam & Abdullahi Anderson Kassimu (2023) Customized structural and mechanical characteristics of Eu^{3+} imbued boro-telluro-dolomite glasses: effect of Dy^{3+} co-doping, Journal of Taibah University for Science, 17:1, 2178165, DOI: 10.1080/16583655.2023.2178165

To link to this article: https://doi.org/10.1080/16583655.2023.2178165

JOURNAL OF TAIBAH UNIVERSITY FOR SCIENCE
2023, VOL. 17, NO. 1, 2178165
https://doi.org/10.1080/16583655.2023.2178165

JTUSCI

Journal of Taibah University for Science

Taylor & Francis
Taylor & Francis Group

OPEN ACCESS Check for updates

Customized structural and mechanical characteristics of Eu^{3+} imbued boro-telluro-dolomite glasses: effect of Dy^{3+} co-doping

Ibrahim Bulus[a,b], Areej S. Alqarni[c,d], Abd Rahman Tamuri[a], S. K. Ghoshal[e], Ibrahim Mohammed Danmallam[a,f] and Abdullahi Anderson Kassimu[g]

[a]Phosphor Research Group, Department of Physics, Faculty of Science, Universiti Teknologi Malaysia, Skudai, Malaysia; [b]Department of Physics, School of Sciences, Kaduna State College of Education Gidan Waya, Kafanchan, Nigeria; [c]Department of Physics, Faculty of Science, Taibah University, Madinah, Saudi Arabia; [d]Department of Physics, College of Science, Princess Nourah bint Abdulrahman University, Riyadh, Saudi Arabia; [e]Advanced Optical Materials Research Group & Laser Centre, Department of Physics, Faculty of Science, Universiti Teknologi Malaysia, Skudai, Malaysia; [f]okoto Energy Research Centre, Usmanu Danfodiyo University, Sokoto, Nigeria; [g]Department of Physics, Faculty of Science, Air Force Institute of Technology (AFIT), Kaduna, Nigeria

ABSTRACT

Inorganic oxide glasses with high mechanical strength and durability became demanding. Thus, a new type of Eu^{3+}/Dy^{3+} co-doped boro-telluro-dolomite glass system with customized structures and mechanical properties were prepared by the melt-quenching method and characterized. The densities, FTIR and Raman spectra of the glasses revealed a significant modification in the network structure with the increase of Dy^{3+} contents. The values of microhardness and elastic moduli of the glasses were increased with the increase of co-doping contents. In addition, a correlation between the glass hardness and applied load was established. The proposed glasses were shown to withstand about 300 g applied force without any distortion, confirming their usefulness to design mechanically stable screen shield and high strength surfaces.

ARTICLE HISTORY
Received 4 November 2022
Revised 19 January 2023
Accepted 2 February 2023

KEYWORDS
Boro–telluro–dolomite glasses; co-doping; network structures; mechanical properties; microhardness

1. Introduction

Nowadays, distinct class of oxide glasses obtained by blending various natural minerals with usual synthetic glass formers has drawn much attention [1–3]. The ever-growing interest on these glasses is mainly due their enhanced chemical and thermal stability, high rare-earth ions (REIs) solubility, and moderate mechanical strength [4,5]. It was reported that any glass host incorporated with natural minerals by virtue of their excellent hardness, high Young's modulus, high fracture toughness together with high resistance against scratches and sharp contact damage find countless applications in the protective covers of electronic displays such as smartphones, laptops, tablets, and wearable devices [6]. Ideally, the cover glasses are the outermost layer of the electronic displays and remain the most vulnerable part of these wearable devices under external force. Extreme hardness and higher Young's modulus can reduce the glass thickness while retaining sufficient durability [7]. Despite the promises of this kind of glass system, nevertheless the selection of abundant minerals that can suitably be amalgamated into the existing synthetic based glass formers to form a new class of glass matrix for the aforementioned usage remains challenging.

Repeated studies showed that the structures, mechanical and optical properties of these glasses can appreciably be improved by europium (Eu^{3+}) and dysprosium (Dy^{3+}) ions co-doping. Besides, efforts have been made to incorporate the dolomite mineral (calcium rich stone) and other by-products such as wollastonite, cement dust, and ashes from sugarcane, coconut husk, palm oil, soda lime silica, and white rice husk into different oxide glass hosts for improving their structural, mechanical and optical performance wherein Abdellaoui et al. [8] studied the influence of natural raw barite and dolomite minerals on the glass forming ability of borate system. The results showed an increase in the glass density, molar volume, and the ratio of BO_4 to BO groups with the increase of BaO contents. Furthermore, the glass transition temperature and optical band gap were decreased, and the UV cut-off was moved towards higher wavelength with the increase of BaO contents. The gamma ray shielding features of lithium borate glasses doped with dolomite, hematite and goethite minerals were also studied [9]. The results revealed much higher increase in the glass density, transparency, exposure buildup factor and radiation shielding properties with the inclusion of dolomite than hematite and goethite.

CONTACT Ibrahim Bulus sibkrishna@utm.my Phosphor Research Group, Department of Physics, Faculty of Science, Universiti Teknologi Malaysia, Skudai, Johor 81310, Malaysia; S. K. Ghoshal ibshekwolo@yahoo.com Advanced Optical Materials Research Group & Laser Centre, Department of Physics, Faculty of Science, Universiti Teknologi Malaysia, Skudai, Johor 81310, Malaysia

Table 1. Glass code, compositions, density (ρ) and molar volume (V_m) of the studied glasses.

	Compositions (mol%)						ρ (g/cm^3)	V_m (cm^3/mol)
Glass codes	B_2O_3	TeO_2	Dp	Dm	Eu_2O_3	Dy_2O_3	±0.003	±0.003
BTDEu0.1Dy	33.9	30	20	15	1.0	0.1	2.310	60.434
BTDEu0.3Dy	33.7	30	20	15	1.0	0.3	2.659	52.859
BTDEu0.5Dy	33.5	30	20	15	1.0	0.5	2.716	51.961
BTDEu0.7Dy	33.3	30	20	15	1.0	0.7	3.024	46.863
BTDEu0.9Dy	33.1	30	20	15	1.0	0.9	3.465	41.078

The elastic and optical properties of CeO_2-doped borotellurite glasses containing two dolomite minerals (pebble and marble) was reported, indicating their usefulness for the development of active filter in optical devices [10]. Zakaly et al. [11] prepared a series of dolomite-borate glasses using the melt-quenching method and determined their physical, structural, and optical characteristics. A comprehensive overview of recent literatures showed that majority of the studies focused on the thermo-luminescence features of these glasses [12–15]. The incorporation of dolomite in the lead-zinc borate glasses was observed to improve their gamma radiation shielding capacity. Despite an excellent shielding potency shown by the glass composed of optimum dolomite content, yet their physical and mechanical properties still need further improvement wherein REIs co-doping may be viable strategy.

The amalgamation of boron oxide having high phonon energy and tellurium oxide with low thermal stability as foundational glass former can impart desired practical properties to the final product like low phonon energy, high thermal stability and negligible hydroscopic nature [16–18]. Moreover, the physical, structural and mechanical properties of La^{3+} infused zinc borate [19], Ag/Eu^{3+}-magnesium zinc sulfophosphate [20] and Nd_2O_3:SrO-Bi_2O_3-B_2O_3 [21] glasses were meaningfully enriched due to the integration of REIs. However, studies on the structural and mechanical properties of Eu^{3+}/Dy^{3+} incorporation in boro-tellurate glass system containing dolomite mineral to the best of authors knowledge has not been reported.

Based on the aforementioned facts, we made a series of Eu^{3+}/Dy^{3+} co-doped boro-telluro-dolomite glasses and determined their structural and mechanical characteristics. The main purpose was to develop a high strength glass system with improved structural and mechanical properties suitable for mobile devices screen protector applications. As-quenched samples were characterized using different analytical instrument to determine some essential parameters like density, molar volume, N_4 ratio, microhardness and elastic moduli. Furthermore, the effects of various Eu^{3+}/Dy^{3+} co-doping concentrations on the network structures and mechanical traits of the boro-telluro-dolomite glasses were examined. The obtained experimental results were analyzed, discussed, and compared with similar findings reported in the state-of-the-art literature.

2. Materials and methods

2.1. Preparation of glass samples

In this study, analytical grade chemical reagents (99.99% purity, Sigma Aldrich) of tellurium dioxide (TeO_2), boron oxide (B_2O_3) europium oxide (Eu_2O_3), dysprosium oxide (Dy_2O_3) oxide and dolomite (CaMg$(CO_3)_2$) were acquired. Dolomite minerals (pebble and marble) were collected from various sites of Johor (Malaysia) and crushed into fine powder using the (100 ×60) Mini-Jaw Crusher. Eu^{3+}/Dy^{3+} co-doped boro-telluro-dolomite (BTD) glasses of composition $(34 - b)$ B_2O_3-TeO_2-20Dp-15Dm-1Eu_2O_3-$b$$Dy_2O_3$ (where $b = 0.3$, 0.3, 0.5, 0.7 and 0.9 mol%, Dp = Dolomite pebble and Dm = Dolomite marble) were made using the conventional melt-quenching route and coded as BTDEu bDy (Table 1). First, about 15 g of the glass constituents (called batch composition) were weighed and homogeneously mixed in an alumina crucible, and melted at 1200°C for 1 h 30 min in a high temperature electrical furnace. Next, the molten fluid was dispensed onto a pre-heated stainless-steel mold and subjected to annealing in another furnace at 400°C for 3 h to release the residual strain that may cause glass embrittlement.

2.2. Characterizations of samples

2.2.1. XRD and SEM-EDX analyses

The amorphous nature of the as-quenched samples was confirmed using X-ray diffraction analyses (Siemens X-Ray Diffractometer D5000 that used Cu-Kα line of wavelength $\approx$ 1.54 Å at 40 kV and 30 mA). The samples' XRD patterns were recorded in the angular (2θ) range of 10° to 80° at scan rate of 2° per minute. The microstructures, surface morphology and presence of chemical elements in the dolomite minerals and samples were examined using the energy dispersive X-ray (EDX, SwiftED3000) spectrometer attached to a table top scanning electron microscope (SEM, TM3000 Hitachi). All the prepared samples were characterized at room temperature.

2.2.2. Density measurement

The density (ρ) of the studied samples was measured using Archimedes principle with distilled water (density, $\rho_W = 1$ gcm^{-3}) as immersion liquid and calculated

using [22]:

$$\rho = \frac{W_a}{W_a - W_b} \times \rho_w \quad (1)$$

where W_a and W_b are the sample's weight in air and water, respectively. The molar volume (V_m) in terms of molecular weight (M_w) of the glass samples were calculated using [23]:

$$V_m = \frac{M_w}{\rho} \quad (2)$$

2.2.3. FTIR and Raman spectral analyses

The FTIR spectra of the prepared samples were recorded in the range of 400–4000 cm^{-1} at a resolution of 4 cm^{-1}. Small amounts of powdered samples were mixed thoroughly with KBr at a ratio of 1:100 mg. The resultant mix was then hard-pressed by 5 ton per square inch pressure for one minute to get a transparent pellet of approximately 1 mm thick. The obtained pellet was used to record the FTIR spectra. The Raman spectra of the glasses in the range of 200–2000 cm^{-1} at a resolution of 1 cm^{-1} were recorded (HR800 UV Horiba Jobin Yvon Raman Spectrometer). FTIR and deconvoluted Raman spectra were used to estimate the N_4 ratio [24]:

$$N_4 = \frac{A_4}{A_4 + A_3} \quad (3)$$

where A_4 and A_3 are the area of the IR and Raman bands in the range of 800-1200 cm^{-1} and 1200-1700cm^{-1} due to the vibration of BO_4 and BO_3 units, respectively.

2.2.4. Vicker's microhardness and ultrasonic velocity test

Micro-indentation measurement was performed on each sample with the applied loads of 50, 100, 200, 300 and 500 g (at a retention time of 15 s) using a digital micro-hardness tester (Shimadzu HVM-2). The values of glass microhardness were estimated using [5]:

$$H_V = 1.854\frac{F}{l^2} \quad (4)$$

where H_V is the Vickers hardness (in Hg/mm^2), F is the applied force (in Newton) and l is the average length (in metres) of the indentation's diagonals.

The longitudinal (V_L) and shear (V_S) ultrasonic velocities in the glasses at resonant frequency of 4 MHz were measured by a Ultrasonic flaw detector (RIGOL DS2202 digital storage oscilloscope). The values of V_L and V_S was calculated using [25]:

$$V_L = \frac{2d}{\Delta t} \quad (5)$$

$$V_S = \frac{2d}{\Delta t} \quad (6)$$

where d is the glass thickness and Δt is the time interval (time taken between the start and retrieval of the pulse appear on the screen during round-trip).

The obtained values of ρ, V_L and V_S were used to estimate the Lame's constants (λ and μ) [26]:

$$\lambda = \rho({V_L}^2 - 2{V_S}^2) \quad (7)$$

$$\mu = \rho {V_S}^2 \quad (8)$$

The values longitudinal (L), shear (G), bulk (K) and Young (E) modulus, Poison ratio (σ) and fractal bond connectivity (D) were evaluated via [26]:

$$L = \lambda + 2\mu \quad (9)$$

$$G = \mu \quad (10)$$

$$L = \lambda + 2\mu \quad (11)$$

$$K = \lambda + \frac{2}{3}\mu \quad (12)$$

$$E = \mu\frac{3\lambda + 2\mu}{\lambda + \mu} \quad (13)$$

$$\sigma = \frac{\lambda}{2(\lambda + \mu)} \quad (14)$$

$$D = \frac{4G}{K} \quad (15)$$

3. Results and discussion

3.1. Physical and structural characteristics of glasses

Figure 1 shows the XRD patterns of the Eu^{3+}/Dy^{3+} co-doped as-quenched samples which did not show any distinct crystalline peaks, rather revealed a broad hump at lower Bragg angles, affirming their amorphous nature. This observation is in agreement with the one reported by Saddeek et. al [27].

Figure 2 displays the EDX spectraand maps of BTDEu0.5Dy glass, indicating the uniform distribution of elements like B, Te, O, C, Ca, Al, Mg, Eu and Dy existed as glass constituents [28]. The white spots in the SEM image (inset of Figure 2(a)) were the artifacts of measurement. The weight percent of the chemical elements were matched to the nominal glass composition (inset

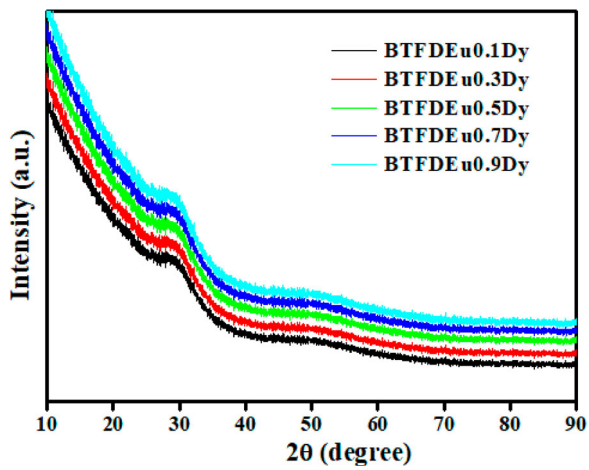

Figure 1. XRD pattern of the as-quenched samples.

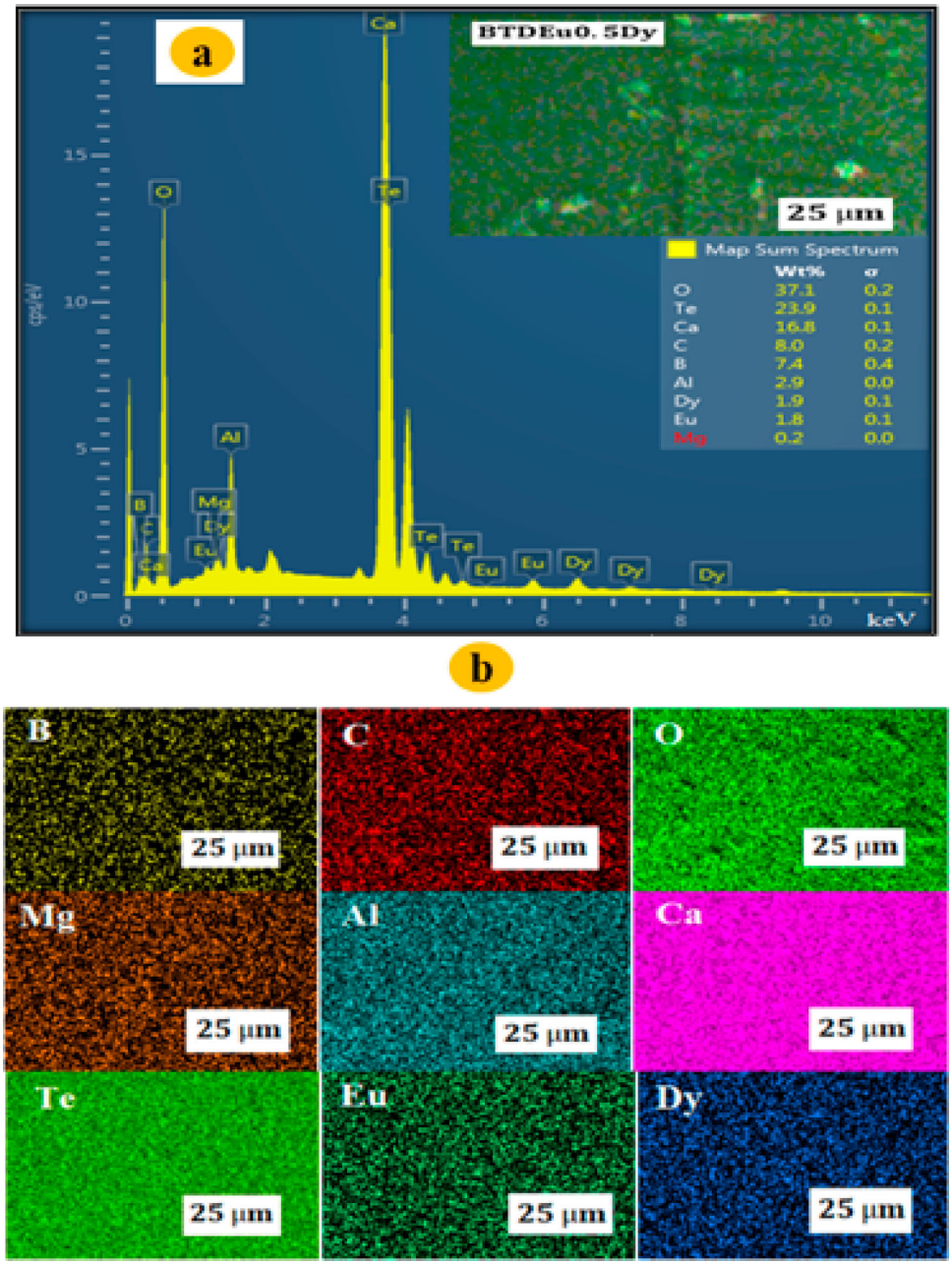

Figure 2. (a) EDX spectra (Inset SEM image and weight percent table) and (b) EDX maps of BTDEu0.5Dy glass.

table of Figure 2(a)). Furthermore, the existence of Al in the studied glass confirmed the successful incorporation of dolomite pebble minerals into the BT glass network.

Figure 3 illustrates the glass density and molar volume as a function of Dy_2O_3 contents. To determine the degree of the geometric configuration, network structures compactness, interstitial space facets and coordination number of the glasses, the density was measured [29]. The REIs concentration dependent variation in the glass density provided a basic insight related to the structural transformation of BO_3 units into four-fold BO_4 units. The numbers of BO_4 structural units were more than BO_3 units, responsible for increasing the network binding and density (more compact structure) of the glasses. The observed increase in the glass density with the increase of Dy_2O_3 contents was mainly due to the replacement of B_2O_3 with lower molecular weight (69.62 g mol^{-1}) by Dy_2O_3 with much higher molecular weight (372.99 $gmol^{-1}$) in the glass matrix. Conversely, the molar volume of the glasses was decreased with an increase of doping levels. Clearly, the inclusion of dopants with higher molecular weight than the host was enabled to increase the density of oxygen packing, transforming the loose network structures of the glass into more compact one [29] useful for the improvement of mechanical performance and durability. The obtained enhancement in the glass density and network structure packing with the increase of Dy_2O_3 contents can be ascribed to the conversion of Sp^2 hybridized planar (triangular) BO_3 units into more stable Sp^3 hybridized BO_4 tetrahedral units. Compared to the

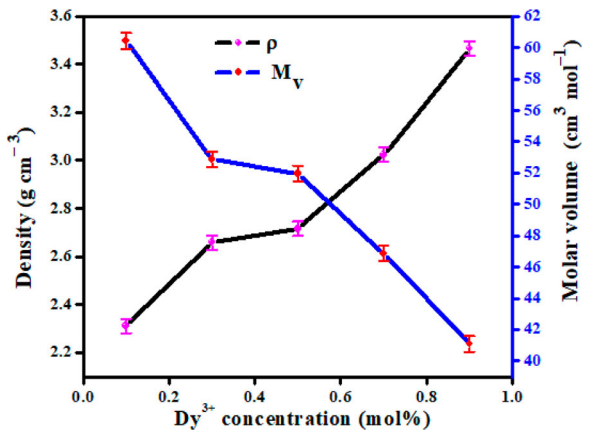

Figure 3. Variation of density and molar volume of the glasses against Dy_2O_3 contents.

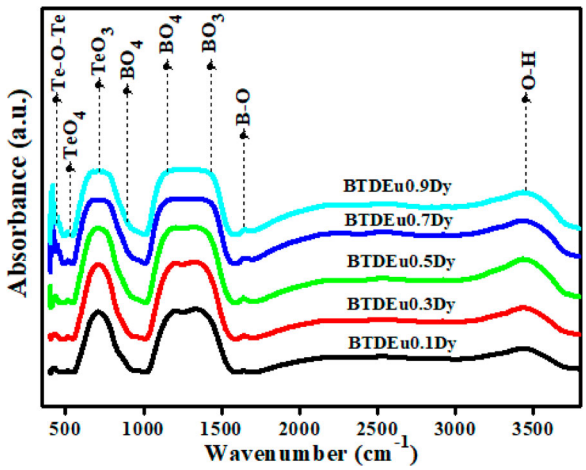

Figure 4. FTIR spectra of the prepared glasses.

planar BO_3 units, BO_4 tetrahedral units are strongly connected together, suggesting a shrinking of the amorphous network structure and thus improvement in the glass density. In addition, the co-dopants (Eu_2O_3 and Dy_2O_3) can occupy the lattice interstitials, leading to a complete modification of the glass network structures [30].

Figure 4 shows the FTIR spectra of the glasses in the range of 380–4000 cm^{-1}. The IR absorption spectral analyses allowed us to distinguish the presence of various chemical functional groups in the proposed glass network. The measured absorbance of the glasses showed the bonding vibrations corresponding to the network former (B_2O_3), conditional network former (TeO_2) and natural minerals (dolomite) network modifier ($MgCa(CO_3)_2$) used in the compositions, wherein the inclusion of co-dopants was found to influence the glass network structures appreciably. However, the IR spectral band positions were not affected significantly with the variation of Dy_2O_3 concentrations. Various literature reports suggested that for any glass host made with B and Te show the IR bands of TeO_4, TeO_3, BO_4 as well as BO_3 units around 600–650, 650–700, 800–1200 and 1200–1400 cm$^{-1,}$ respectively [31]. Herein, the bands

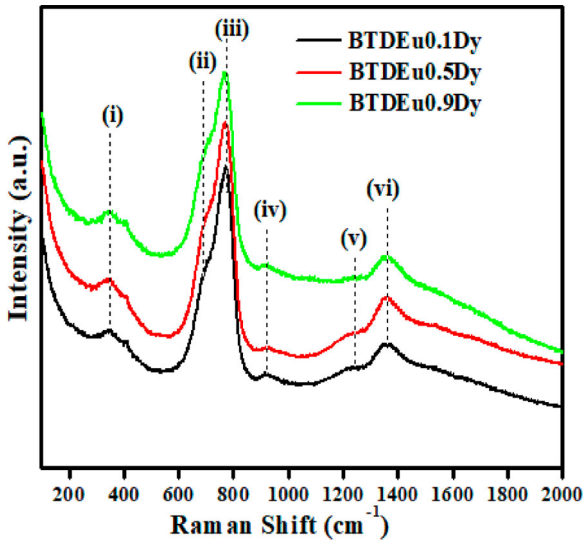

Figure 5. Raman spectra of the selected glasses.

around 403–412 cm^{-1} were due to the bending vibration of Te-O-Te or O-Te-O linkages formed by sharing the corners of TeO_4 and TeO_{3+1} polyhedral units with TeO_3 groups [32]. The FTIR bands at 486–510, 689–726, 951–981, 1144–1200, and 1344–1375 cm^{-1} corresponded to the vibrations of TeO_4, TeO_3, BO_4 and BO_3 structural units [33]. Earlier study reported that pure borate shows a sharp IR peak at 806 cm^{-1} due to the vibration of boroxol ring [34]. However, we did not observe the IR band corresponding to the boroxol ring vibration, indicating the dominance of BO_3 and BO_4 structural units in the proposed glass network. The band at 1630–1667 cm^{-1} was due to the stretching vibration of B-O bonds from isolated pyroborate groups. The IR band at 3444–3469 cm^{-1} was to the stretching vibration of H–O linkage from hydroxyl groups [35].

Figure 5 displays the Raman spectra of some selected samples in the range of 2000–200 cm^{-1}. The Raman analysis complemented the IR results because some of the forbidden transitions in the IR absorbance (zero net dipole moment) became allowed in the Raman spectra due to nonzero net polarizability [36]. Table 2 shows the Raman peak positions and their assignments. The overall Raman profiles for different glasses remain similar wherein the shift in the Raman peak positions with the increase of Dy_2O_3 content was insignificant. The observed peak at 349 cm^{-1} was due to the vibrations of the Te-O bonds from TeO_4 tetrahedra characteristic of α-TeO_2 [37]. The weak peak (shoulder) at 682-696 cm^{-1} was due to the vibrations of Te–O linkages among TeO_4 units and bridging oxygen (BOx) [38]. In addition, the intense Raman peak at 770 cm^{-1} was due to the symmetrical and asymmetrical vibration modes of (Te_{eq}-O) in TeO_{3+1} or TeO_3 units [39]. The weak Raman peak at 922 cm^{-1} was due to the stretching vibration of BO_4 unit from diborate ($B_2O_5{}^{-4}$) groups [40]. The extremely weak peak at 1220 cm^{-1} for all the studied glasses corresponded to the stretching vibration of BO_4 groups.

Table 2. Comparison of the obtained Raman peak positions and assignments with other studies.

Raman shift (cm^{-1})	Reported values (cm^{-1})	Assignment	Ref.
349 (i)	345	Oscillations of TeO bonds inTeO_4 tetrahedra characteristic of α-TeO_2.	[42]
687 (ii)	670–684	Symmetric stretching vibrations of TeO in TeO_4 units or Te–O–Te linkages between two fourfold coordinated Te atoms.	[43]
770 (iii)	750–760	Stretching vibrations of Te–O in TeO_3 units and/or TeO_{3+1} groups.	[43]
922 (iv)	906	B-O stretching vibration in the BO_4 units.	[44]
1220 (v)	1136	Vibrations of pyroborate groups ($B_2O_5^{4-}$).	[45]
1357 (vi)	1311	Vibrations of BO_3 segments	[45]

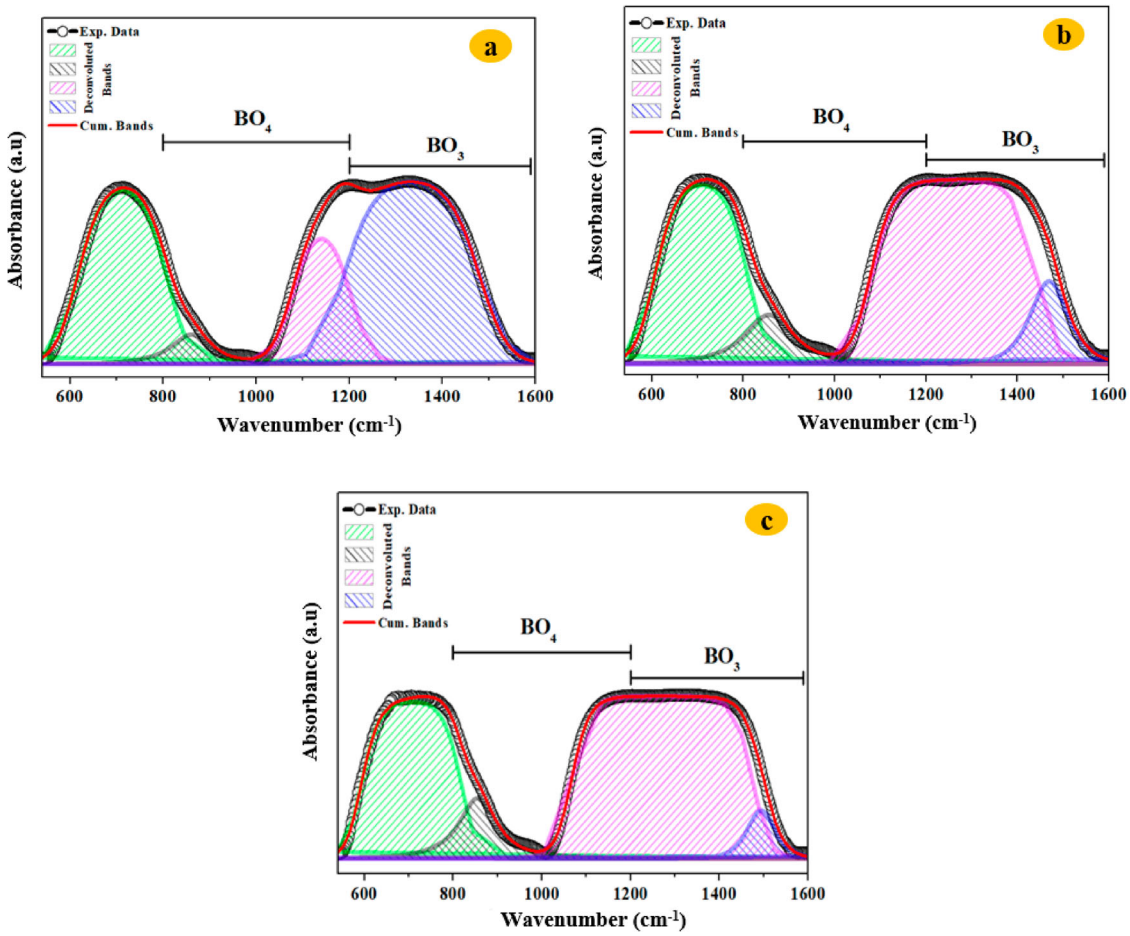

Figure 6. Deconvoluted FTIR spectra of (a) BTDEu0.3Dy, (b) BTDEu0.5Dy and (c) BTDEu0.7Dy glass fitted to Gaussian-Lorentzian function.

The Raman peak at1357 cm^{-1} was due to the asymmetrical stretching vibration of BO_3 groups in different borate units [41]. In brief, both FTIR and Raman spectra of the glasses showed the existence of functional chemical groups of boron and tellurium in the network structures and did not reveal any spectrum related to Dy_2O_3.

Some significant FTIR and Raman spectral peaks were deconvoluted into many Gaussian functions (Figures 6 and 7) to assess the relative area (A) of each component proportional to the structural group abundance [46]. The fraction of the 4-coordinated boron atoms (N_4) was evaluated using the expression described in Section 2.5. Together with the N_4 ratio, the vibrational spectral deconvolution provided a deeper insight into glass network structure whether densely packed or loosely bound matrix. The relative areas of the bands due to the IR vibration of BO_4 units in the range of 800–1200 cm^{-1} (A_4), BO_3 units in the range of 1200–1600 cm^{-1} (A_3), TeO_4 units (in the range of 600–650 cm^{-1}) and TeO_3 units (in the range of 650–800 cm^{-1}) were calculated. Table 3 shows the achieved relative areas and N_4 ratio of the glasses.

Figure 8 illustrates the Dy_2O_3 contents dependent N_4 and TeO_4 ratio in the glasses. The N_4 ratio was increased gradually with the increase of Dy_2O_3 contents in the glass, indicating an improvement in the glass network compactness through $BO_3 + O \rightarrow BO_4$

Table 3. Relative area of the deconvoluted FTIR and Raman bands alongside N_4.

	Relative area of the deconvoluted FTIR bands centred at			
Glass codes	865 cm^{-1}	1140 cm^{-1}	1339 cm^{-1}	N_4 ratio
BTDEu0.1Dy	4.55	15.94	49.28	0.294
BTDEu0.3Dy	3.67	16.30	48.63	0.291
BTDEu0.5Dy	6.47	55.18	7.79	0.888
BTDEu0.7Dy	7.01	58.53	3.71	0.946
BTDEu0.9Dy	6.93	55.18	7.10	0.897

	Relative area of the deconvoluted Raman peaks						
Glass codes	(i)	(ii)	(iii)	(iv)	(v)	(vi)	N_4 ratio
BTDEu0.1Dy	6.00	53.54	29.62	1.61	1.17	8.07	0.64
BTDEu0.5Dy	7.30	53.96	27.72	1.19	0.76	9.08	0.66
BTDEu0.9Dy	8.69	55.77	25.76	0.76	0.82	8.19	0.68

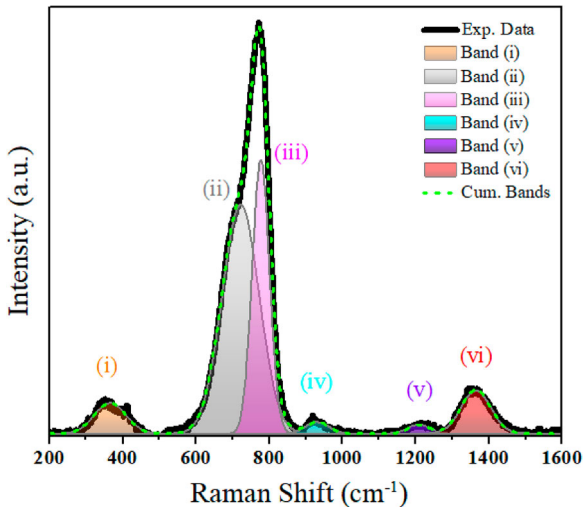

Figure 7. Deconvoluted Raman spectra of a selected glass.

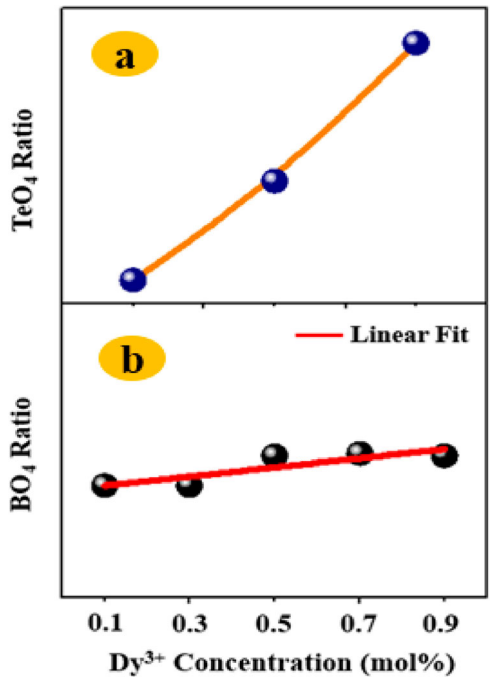

Figure 8. Dy ions contents dependent (a) TeO_4 ratio and (b) N_4 ratio of the studied glasses obtained from FTIR and Raman analysis.

and $TeO_3 + O \rightarrow TeO_4$ isomerization reaction with the generation of more BOx at the expense of non-bridging oxygen (NBOx). Comparable observations were made for the fluoride borate glasses [47] and nickel-doped bismuth borate glasses [48]. It was shown that by tuning the doping contents, the relative fraction of BO_4 and TeO_4 units in the studied glasses can be increased, enabling better control on the glass network structure, density and mechanical performance.

3.2. Mechanical characteristics of glasses

The glass-based screen protectors of various portable electronic devices must be thin, high strength, durable, and light-weight [49]. These glasses should be resilient to external applied stress wherein their resistance to external pressure (shock shielding capacity) can be gauged through the mechanical hardness and elastic moduli measurement. Microhardness test provides basic knowledge on the glass resistance to permanent distortion stimulated via harder materials when subjected to stress. In the present study, the capacity of the proposed glass system in resisting plastic or permanent distortion under intense mechanical loading was examined using the Vickers hardness test [50]. The hardness (H_V) of the glasses were measured at various applied loads (50, 100, 200, 300 and 500 g) with retention time of 15 s. The glass hardness was increased with the decrease of Dy_2O_3 contents as shown in Figure 9. This observed increase in microhardness can be ascribed to the enhancement of glass network rigidity due to the reduction of NBO.

The results (Figure 9) of hardness against applied load can be interpreted by diving into two regions AB (with lower loads) and BC (with higher loads). The region AB is predominantly an active zone wherein the stress–strain behaviour is nonlinear. Conversely, the region BC is essentially a plateau or saturation zone in which the stress–strain response is somewhat independent of the loads variation. The observed non-linear response at lower load was mainly due to the increase of glass resistance toward additional indentations wherein some newly formed dislocations may be nucleated at

Table 4. Ultrasonic velocities, elastic modulus, Poisson ratio and fractal bond connectivity of the present glass system compared to other reported works.

	Ultrasonic velocities (m/s)		Elastic moduli (GPa)				Poison ratio	Fractal bond connectivity	
Glass system	V_L	V_S	L	G	K	E	σ	D	Ref.
BTDEu0.1Dy	5051	2575	58.934	15.317	38.511	40.572	0.324	1.591	Present
BTDEu0.3Dy	5125	2640	69.840	18.532	45.131	48.902	0.319	1.643	Present
BTDEu0.5Dy	5340	2855	77.448	22.138	47.931	57.160	0.300	1.847	Present
BTDEu0.7Dy	5512	2967	91.876	26.621	56.381	69.003	0.296	1.889	Present
BTDEu0.9Dy	5589	3010	108.236	31.393	66.379	81.354	0.295	1.892	Present
Borotellurite	3662	2200	43.02	22.32	15.53	37.81	0.218	–	[54]
Bismuth borotellurite	4328	2417	75.1	23.4	43.9	59.7	0.27	–	[55]
Silica borotellurite	6774	4183	182.6	69.7	89.7	186.0	0.192	–	[56]
Tellurite	3482	1987	68.88	36.14	20.80	52.36	0.25	–	[57]

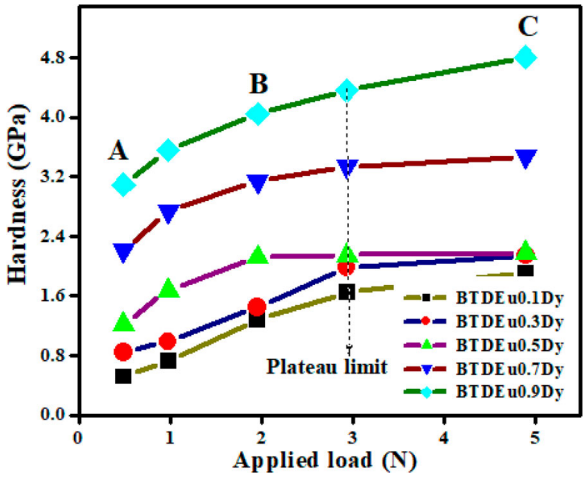

Figure 9. Glass hardness against applied load.

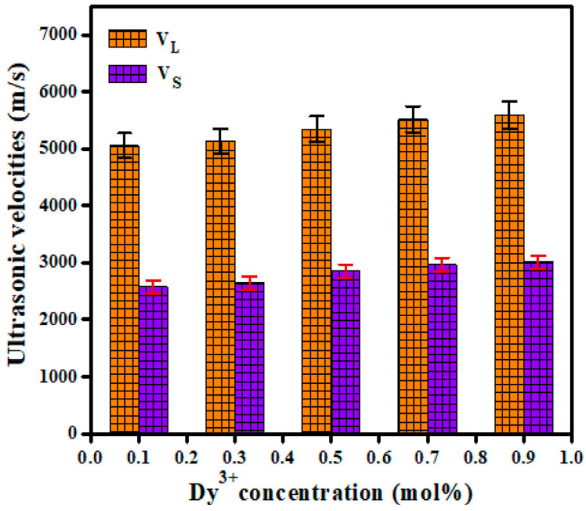

Figure 10. Variation of glass ultrasonic velocities against Dy_2O_3 contents.

the indentation region, thus enhancing the microhardness. The plastic zone (active region) was extended up to 3 N of load matching the plateau limit of the glass hardness. Furthermore, an additional increase in the applied load could lead to the phonon modes softening of the glass, making the microhardness constant. This result indicated that the proposed glass composition can resist up to 300 g (3 N) of applied load without being permanently deformed, making them potential candidates for high performance glass protector in mobile devices.

Deeper insight into the elastic modulus of various glass hosts became significant for the design and fabrication of high strength and durable screen shield [51]. Thus, various elastic parameters of the studied glasses were recorded and compared with the existing-state-of-the-art glass hosts reported in the literature (Table 4). The values of V_L and V_S of the glasses were increased with the increase of Dy_2O_3 concentrations (Figure 10), confirming the increase of glass network compactness and rigidity. In is worth noting that with the increase of glass density, the values of V_L and V_S for most materials generally show a significant increase [52], thus the proposed glasses followed the expected trend. This observation was supported by the improvement of the glass elastic moduli (L, G, K, and E) with the increase of Dy_2O_3 contents (Figure 11). Yet again, the achieved improvement in the elastic moduli of the prepared glass system indicated their good mechanical stability which agreed with the other reported findings on borotellurite glass [53]. It was argued that the observed increase in both ultrasonic velocities and elastic moduli of the glasses with the increase of doping levels was mainly due to the continuous conversion of TeO_3, and BO_3 groups into TeO_4 and BO_4 groups and thereupon the generation of more BOx at the cost of NBOx reduction. In short, the BOx atoms generated from the conversion of BO_3 into BO_4 structural units in turn strengthen the network bonding and density of the cross-links among different constituent atoms in the glass matrix, significantly improving the glass network rigidity and mechanical qualities. These data supported the results of density, FTIR and Raman spectra.

The variation in the Poisson's ratio (σ) with the increase of Dy_2O_3 contents clearly reflected the glass network structures modification (called dimensionality changes) in terms of cross-linking density. Eevon et al. [58] reported that the Poisson's ratio changes can be a good indicator for the glass network structure alterations. A glass system with σ values in the range of 0.1 to

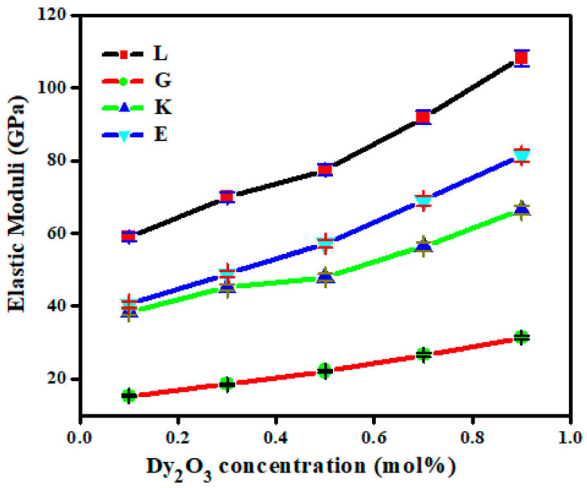

Figure 11. Variation of glass elastic moduli against Dy_2O_3 contents.

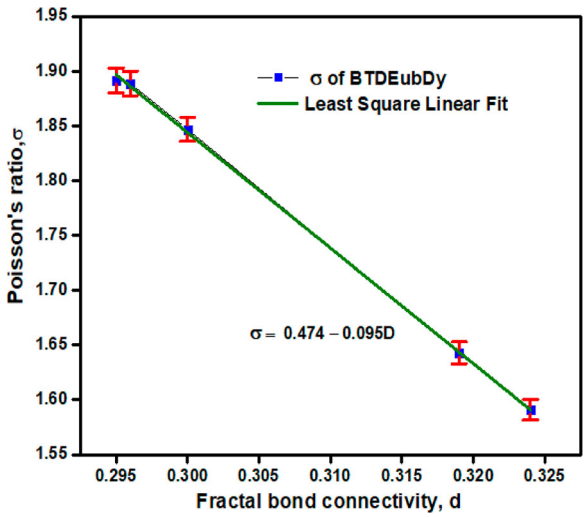

Figure 12. Correlation between the fractal bond connectivity and Poisson's ratio of the produced BTDEubDy glass system.

0.2 is characterized as dense cross-linked network. Conversely, a glass system with σ values in the range of 0.3 to 0.5 is characterized as low density cross-linked network structure. According to Bergman and Kantor [59], fractal bond connectivity (D) can elucidate the effectual dimensionality of a specific material (for example inhomogeneous random mix of fluid states and solid backbones) near the percolation threshold. Interestingly, the value of D for the network structures in 1D, 2D and 3D are approximately 1.0, 2.0 and 2.0, respectively. In the current glasses, the values of σ was ≥ 0.3, indicating their low cross-linking network density. In addition, the values of D of the studied glasses were found to be 2.0, confirming their 2D network structures.

Figure 12 depicts the correlation between fractal bond connectivity and Poisson's ratio of the glasses. In pure B_2O_3 glass, most of the triangular BO_3 units are organized as boroxol rings wherein 3 O atoms are within the ring and 3 O atoms occur at the exterior of the ring. When the BO_3 units undergo constant transformation into BO_4 units due to the addition of Dy_2O_3 as substitute of B_2O_3, these boroxol rings suffer random interconnections. Consequently, the values of Poisson ratio decrease and dimensionality of glass network increase (Table 4). This observation is consistent with the proposed semi-empirical relation $\mu = A - zD$ [59]. The obtained $\sigma - D$ correlation was fitted to $\sigma = 0.474 - 0.095D$, with correlation constant of 0.09, wherein the constants A and z validated the earlier claim made from the study on the WO_3–B_2O_3–MgO–TeO_2 glass system with $\sigma = 0.466 - 0.09D$ [60], oxyfluorozinc-tellurite with $\sigma = 0.45 - 0.083D$ [61] and oxyfluoride tellurite AlF3-ZnO-TeO_2 with $\sigma = 0.54 - 0.085$ [62].

4. Conclusion

The possibility of customizing the structure and mechanical properties of some newly developed boro-tellurodolomite glasses by co-doping with Eu_2O_3/Dy_2O_3 was determined for the first time. These glasses of composition $(34 - b)$ B_2O_3-TeO_2-20Dp-15Dm-1Eu_2O_3-bDy_2O_3 (where b =0.1, 0.3, 0.5, 0.7 and 0.9 mol%) were made using melt-quenching method and thoroughly characterized. The incorporation of Dy_2O_3 into the glass matrix was found to appreciably enhance the glass stiffness without affecting the borate entities, leading to an increase in the density and network compactness, thus improving the mechanical qualities useful for high performance screen shield. The FTIR and Raman spectral deconvolution confirmed a significant improvement in the structural and mechanical characteristics of the glassed due to Eu_2O_3/Dy_2O_3 concentration tuning, wherein the N_4 ratio was shown to increase. This structural enhancement of the glasses was ascribed to the isomerization process of $BO_3 + NBOs \leftrightarrow BO_4$ and $TeO_3 + O \rightarrow TeO_4$. The high elastic modulus and strong correlation between fractal bond connectivity and Poisson's ratio of the glasses affirmed their high resistance against permanent deformation under external applied pressure, making them protective for mobile devices screen protector.

Disclosure statement

No potential conflict of interest was reported by the author(s).

ORCID

S. K. Ghoshal http://orcid.org/0000-0002-3180-6790

References

[1] Kara U, Kavaz E, Issa SA, et al. Optical, structural and nuclear radiation shielding properties of $Li_2B_4O_7$ glasses: effect of boron mineral additive. Appl Phys A. 2020;126(4):1–17.

[2] Kara U, Issa SA, Susoy G, et al. Synergistic effect of serpentine mineral on $Li_2B_4O_7$ glasses: optical, structural and nuclear radiation shielding properties. Appl Phys A. 2020;126(3):1–19.

[3] Acikgoz A, Ceyhan G, Aktas B, et al. Luminescent, structural and mechanical properties of erbium oxide doped natural obsidian glasses. Journal of Non-Crystalline Solids. 2021;572:121104.
[4] Hou G, Cao L, Zhang C, et al. Improving mechanical strength of La_2O_3 and ZrO_2 co-doped silicate glasses for touch screen. Funct Mater Lett. 2018;11(2):1850026.
[5] Sani G, Limbach R, Dellith J, et al. Surface damage resistance and yielding of chemically strengthened silicate glasses: from normal indentation to scratch loading. J Am Ceram Soc. 2021;104(7):3167–3186.
[6] Guo Y, Li J, Zhang Y, et al. High-entropy R_2O_3-Y_2O_3-TiO_2-ZrO_2-Al_2O_3 glasses with ultrahigh hardness. Young's modulus, and indentation fracture toughness. Iscience. 2021;24(7):102735.
[7] Lin G, Huang Y. High mechanical strength sapphire cover lens for smartphone screen. Crystal Res Technol. 2018;53(7):1800049.
[8] Abdellaoui K, Ratep A, Boumaza A, et al. The effect of the natural raw barite and the dolomite material on borate glass formation. J Fundam Appl Sci. 2018;10(1): 281–300.
[9] Kavaz E. An experimental study on gamma ray shielding features of lithium borate glasses doped with dolomite, hematite and goethite minerals. Radiat Phys Chem. 2019;160:112–123.
[10] Bulus I, Hussin R, Ghoshal SK, et al. Enhanced elastic and optical attributes of boro-telluro-dolomite glasses: role of CeO_2 doping. Ceram Int. 2019;45(15):18648–18658.
[11] Zakaly HM, Rashad M, Tekin HO, et al. Synthesis, optical, structural and physical properties of newly developed dolomite reinforced borate glasses for nuclear radiation shielding utilizations: an experimental and simulation study. Opt Mater. 2021;114:110942.
[12] Fernandes BG, Cano NF, Rao TG, et al. Thermoluminescence and optical absorption properties of glass from natural diopside and of synthetic diopside glass. J Non Cryst Solids. 2017;456:22–26.
[13] Kavaz E, Yorgun NY. Gamma ray buildup factors of lithium borate glasses doped with minerals. J Alloys Comp. 2018;752:61–67.
[14] Yorgun NY. Gamma-ray shielding parameters of $Li_2B_4O_7$ glasses: undoped and doped with magnetite, siderite and Zinc-Borate minerals cases. Radiochim Acta. 2019; 107(8):755–765.
[15] Akça-Özalp S, Portakal-Uçar ZG, Oğlakçı M, et al. Characterization of thermoluminescence kinetic parameters of dolomite after exposure to β-radiation dose. J Lumines. 2021;240:118427.
[16] Teresa PE, Naseer KA, Marimuthu K, et al. Influence of modifiers on the physical, structural, elastic and radiation shielding competence of Dy^{3+} ions doped alkali boro-tellurite glasses. Radiat Phys Chem. 2021;189: 109741.
[17] Devaraja C, Gowda GJ, Eraiah B, et al. Structural, conductivity and dielectric properties of europium trioxide doped lead boro-tellurite glasses. J Alloys Comp. 2022;898:162967.
[18] Mallur SB, Babu PK. Optical properties of praseodymium (Pr^{3+}) doped bismuth boro-tellurite glasses containing CdSe nanoparticles. Mater Res Bull. 2022;147: 111651.
[19] Januchta K, Youngman RE, Jensen LR, et al. Mechanical property optimization of a zinc borate glass by lanthanum doping. J Non Cryst Solids. 2019;520:119461.
[20] Danmalam IM, Bulus I. Correlation of optical and mechanical properties of silver nanoparticles sensitized europium doped magnesium zinc sulfophosphate glasses. Sci Proc Series. 2020;2(2):147–155.
[21] Gaafar MS, Marzouk SY, Mahmoud IS, et al. Role of neodymium on some acoustic and physical properties of Bi_2O_3-B_2O_3-SrO glasses. J Mater Res Technol. 2020;9(4):7252–7261.
[22] Gaikwad DK, Sayyed MI, Botewad SN, et al. Physical, structural, optical investigation and shielding featuresof tungsten bismuth tellurite based glasses. J Non Cryst Solids. 2019;503:158–168.
[23] Bulus I, Dalhatu SA, Hussin R, et al. The role of dysprosium ions on the physical and optical properties of lithium-borosulfophosphate glasses. Int J Modern Phys B. 2017;31(13):1750101.
[24] Elkhoshkhany N, Samir N. Structural, thermal and optical properties of oxy-fluoro borotellurite glasses. J Mater Res Technol. 2020;9(3):2946–2959.
[25] El-Mallawany R, Afifi HA, El-Gazery M, et al. Effect of Bi_2O_3 addition on the ultrasonic properties of pentaternary borate glasses. Measurement. 2018;116:314–317.
[26] Ouis MA, Taha MA, El-Bassyouni GT, et al. Thermal, mechanical and electrical properties of lithium phosphate glasses doped with copper oxide. Bull Mater Sci. 2019;42(5):1–10.
[27] Saddeek YB, Aly KA, Shaaban KS, et al. Physical properties of B_2O_3–TeO_2–Bi_2O_3 glass system. J Non Cryst Solids. 2018;498:82–88.
[28] Szal R, Zmojda J, Kochanowicz M, et al. Spectroscopic properties of antimony modified germanate glass doped with Eu^{3+} ions. Ceram Int. 2019;45(18):24811–24817.
[29] Singh GP, Kaur P, Kaur S, et al. Investigation of structural, physical and optical properties of CeO_2–Bi_2O_3–B_2O_3 glasses. Phys B Condens Matter. 2012;407(21):4168–4172.
[30] Shamshad L, Ali N, Kaewkhao J, et al. Luminescence characterization of Sm^{3+}-doped sodium potassium borate glasses for laser application. J Alloys Comp. 2018;766: 828–840.
[31] Kaur A, Khanna A, Bhatt H, et al. BO and TeO speciation in bismuth tellurite and bismuth borotellurite glasses by FTIR, 11B MAS-NMR and Raman spectroscopy. J Non Cryst Solids. 2017;470:19–26.
[32] Kaur A, Khanna A, Krishna PSR, et al. Structure of copper tellurite and borotellurite glasses by neutron diffraction. Raman(11B). MAS-NMR and FTIR spectroscopy. Phys Chem Glasses Eur J Glass Sci Technol Part B. 2020;61(1):27–39.
[33] Rani S, Ahlawat N, Parmar R, et al. Role of lithium ions on the physical, structural and optical properties of zinc boro tellurite glasses. Indian J Phys. 2018;92(7):901–909.
[34] Asyikin AS, Halimah MK, Latif AA, et al. Physical, structural and optical properties of bio-silica borotellurite glass system doped with samarium oxide nanoparticles. J Non Cryst Solids. 2020;529:119777.
[35] Kaky KM, Lakshminarayana G, Baki SO, et al. Structural, thermal, and optical analysis of zinc boro-aluminosilicate glasses containing different alkali and alkaline modifier ions. J Non Cryst Solids. 2017;456:55–63.
[36] Abdullahi I, Hashim S, Ghoshal SK, et al. Structures and spectroscopic characteristics of barium-sulfur-telluroborate glasses: role of Sm^{3+} and Dy^{3+} Co-activation. Mater Chem Phys. 2020;247:122862.
[37] Yadav AK, Singh P. A review of the structures of oxide glasses by Raman spectroscopy. RSC Adv. 2015;5(83): 67583–67609.
[38] Sailaja P, Mahamuda S, Talewar RA, et al. Spectroscopic investigations of dysprosium ions doped oxy chloro boro

tellurite glasses for visible photonic device applications. J Alloys Comp. 2019;789:744–754.
[39] Mohamad Azaludin NR, Sabri NS. Infrared spectroscopy of mixed glass former effect in borotellurite glasses: a review. Gading J Sci Technol. 2021;4(1):94–102.
[40] Krishna VM, Mahamuda S, Talewar RA, et al. Dy^{3+} ions doped oxy-fluoro boro tellurite glasses for the prospective optoelectronic device applications. J Alloys Comp. 2018;762:814–826.
[41] Naresh P, Kavitha B, Inamdar HK, et al. Modifier role of ZnO on the structural and transport properties of lithium boro tellurite glasses. J Non Cryst Solids. 2019;514:35–45.
[42] Sangeetha G, Sekhar KC, Hameed A, et al. Influence of CaO on the structure of zinc sodium tetra borate glasses containing Cu^{2+} ions. J Non Cryst Solids. 2021;563: 120784.
[43] García-Amaya IV, Zayas ME, Alvarado-Rivera J, et al. Spectroscopic studies of the behavior of Eu on the luminescence of cadmium tellurite glasses. J Spectr. 2015; 2015.
[44] Pandarinath MA, Upender G, Rao KN, et al. Thermal, optical and spectroscopic studies of boro-tellurite glass system containing ZnO. J Non Crystall Solids. 2016;433:60–67.
[45] Yaacob SS, Sahar MR, Mohd-Noor F, et al. The effect of Nd_2O_3 content on the properties and structure of Nd^{3+} doped TeO_2–MgO–Na_2O-glass. Optical Mater. 2021;111:110588.
[46] Alqarni AS, Hussin R, Alamri SN, et al. Tailored structures and dielectric traits of holmium ion-doped zinc-sulpho-boro-phosphate glass ceramics. Ceram Int. 2020;46(3): 3282–3291.
[47] ElBatal FH, Abdelghany AM, ElDin FE, et al. Vanadium structural role in binary fluoride borate glasses and effects of gamma irradiation. Radiat Phys Chem. 2020;170:108659.
[48] Thakur S, Thakur V, Kaur A, et al. Structural, optical and thermal properties of nickel doped bismuth borate glasses. J Non Cryst Solids. 2019;512(9):60–71.
[49] Barlet M, Delaye JM, Charpentier T, et al. Hardness and toughness of sodium borosilicate glasses via Vickers's indentations. J Non Cryst Solids. 2015;417:66–79.
[50] Ren M, Cheng JY, Jaccani SP, et al. Composition–structure–property relationships in alkali aluminosilicate glasses: a combined experimental–computational approach towards designing functional glasses. J Non Crystall Solids. 2019;505:144–153.
[51] Elokr M, AbouDeif Y. Optical, elastic properties and DTA of TNZP host tellurite glasses doped with Er3 + ions. J Mol Struct. 2016;1108:257–262.
[52] Lee CS, Matori KA, Ab Aziz SH, et al. Comprehensive study on elastic moduli prediction and correlation of glass and glass ceramic derived from waste rice husk. Adv Mater Sci Eng. 2017;2017.
[53] Zaitizila I, Halimah MK, Muhammad FD, et al. Influence of manganese doping on elastic and structural properties of silica borotellurite glass. J Non Cryst Solids. 2018;492:50–55.
[54] Halimah MK, Umar SA, Chan KT, et al. Study of rice husk silicate effects on the elastic, physical and structural properties of borotellurite glasses. Mater Chem Phys. 2019;238:121891.
[55] El-Gazery M, Ali A, El-Mallawany R. Ultrasonic and thermal properties of bismuth borotellurite glasses doped with $NdCl_3$. Egypt J Chem. 2019;62(4):655–664.
[56] Nor NM, Kamari HM, Latif AA, et al. Elastic properties of vanadium doped silica-borotellurite glasses. Solid State Phenom. 2020;307:321–326.
[57] Tafida RA, Halimah MK, Muhammad FD, et al. Structural, optical and elastic properties of silver oxide incorporated zinc tellurite glass system doped with Sm^{3+} ions. Mater Chem Phys. 2020;246:122801.
[58] Eevon C, Halimah MK, Azmi Z, et al. Elastic properties of TeO_2-B_2O_3—ZnO-Gd_2O_3 glasses using non-destructive ultrasonic technique. Chalcog Lett. 2016;13(6):281–289.
[59] Bergman DJ, Kantor Y. Critical properties of an elastic fractal. Phys Rev Lett. 1984;53(6):511.
[60] Abd El-Moneim A, El-Mallawany R. Analysis and prediction for elastic properties of quaternary tellurite Ag_2O–V_2O_5–MoO_3–TeO_2 and WO_3–B_2O_3–MgO–TeO_2 glasses. J Non Crystall Solids. 2019;522:119580.
[61] Abd El-Moneim A. Oxyfluoro-zinc-tellurite glasses–part I: predicting the elastic properties and glass transition temperature under the substitution of AlF3 by ZnO. J Fluor Chem. 2019;217:97–104.
[62] El-Moneim AA. An extensive study on the prediction of elastic properties in oxyfluoride tellurite AlF3–ZnO–TeO2 glasses under the substitution of TeO_2 by AlF_3. Phys Chem Glass Eur J Glass Sci Technol Part B. 2019;60(5): 203–211.